Solstice optimizes thermal growing season
Supplementary materials

Victor, Lizzie

Aug.-Dec. 2024

Supplementary methods

All analyses were run on **R**, using the package `terra` for raster manipulation (Hijmans, 2024). The workflow of the analysis is represented in the Figure S1.

Climate data We extracted daily mean temperatures, from 1951 to 2020, from the ERA5-Land dataset, at a 0.1° spatial resolution (Muñoz Sabater et al., 2021). We sampled >500 sites on a regular grid across Europe (see Figure 2 in the main text).
Following McMaster and Wilhelm (1997), we define growing degree-days at a day d (GDD_d) as:

$$GDD_d = \begin{cases} 0 & \text{if } T_d < T_{lower} \\ T_{upper} - T_{lower} & \text{if } T_d > T_{upper} \\ T_d - T_{lower} & \text{otherwise} \end{cases} \tag{1}$$

where T_d is the mean temperature at the day d, and T_{lower}/T_{upper} the lower/upper temperature thresholds (defining the range within which metabolism is likely active). Here, we chose $T_{lower} = 5°C$ and $T_{upper} = 35°C$ (see Figure S2 for the same analysis with 0-40°C range).

Optimal period For each day and each site, we computed environmental predictability as the R^2 of the linear regression across years between total GDD and the GDD accumulated by that day (blue panel, Figure S1). Growth potential was defined as the remaining GDD to be accumulated from that day until the end of the year (yellow panel, Figure S1). While other trade-offs could be considered, we chose this as the simplest option (and perhaps most obvious), especially given our limited understanding of the underlying loss functions plants may rely on. We computed both environmental predictability and growth potential for the entire year (January 1 to December 31), although the growing season is likely more restricted and varies across locations.
We computed an optimality measure based on the Euclidean distance D from the ideal point where both predictability and growth potential (scaled to $[0, 1]$) are maximized (green panel, Figure S1). Optimality was defined as $max(D) - D$ (where $max(D)$ is the Euclidean distance between the point $(0, 0)$ and the point $(1, 1)$, i.e. $max(D) = \sqrt{1^2 + 1^2} \approx 1.414$)—such that higher values correspond to more optimal days. Days were classified as optimal if they fell within the top 10% of days with the higher optimality.
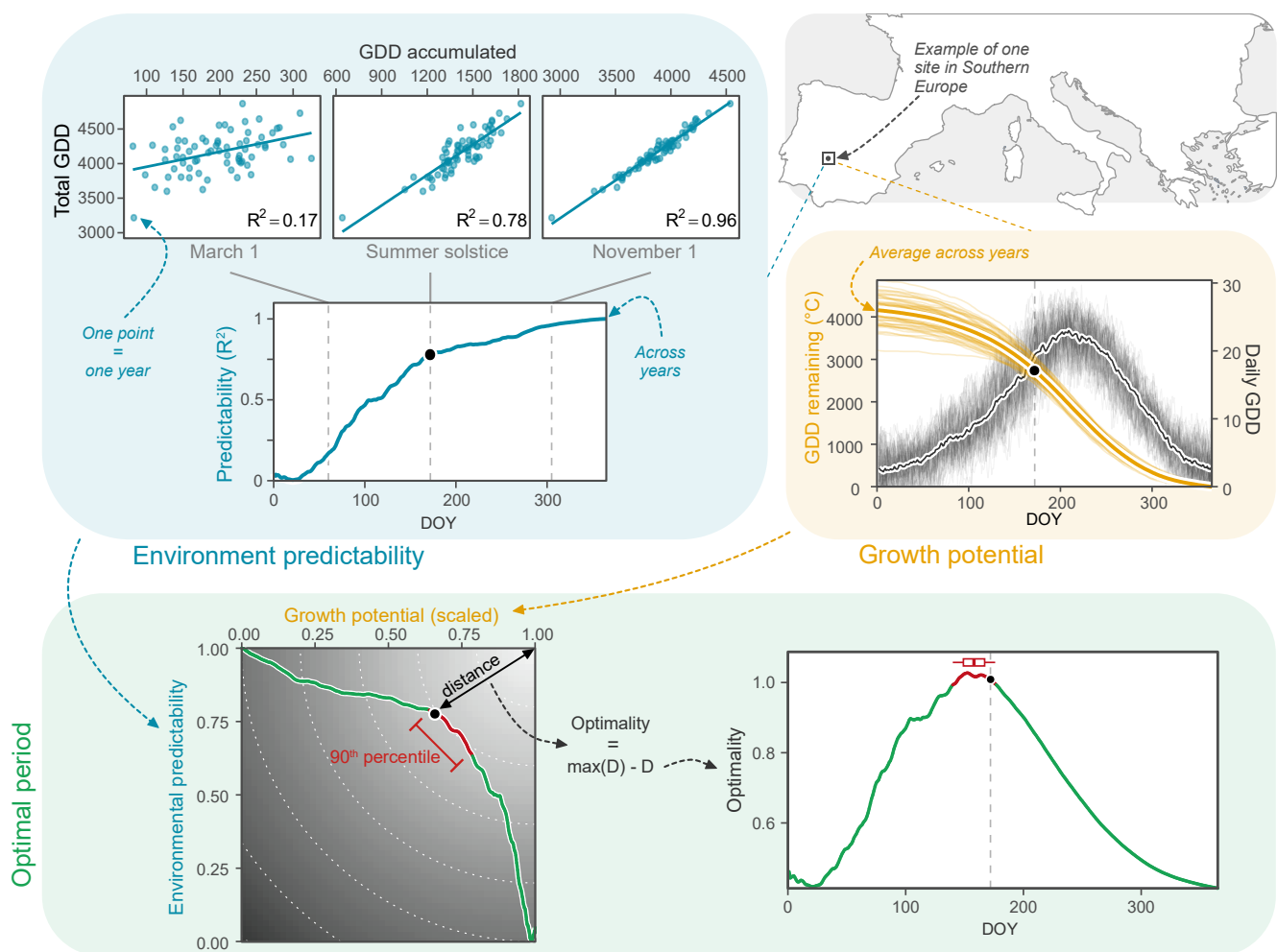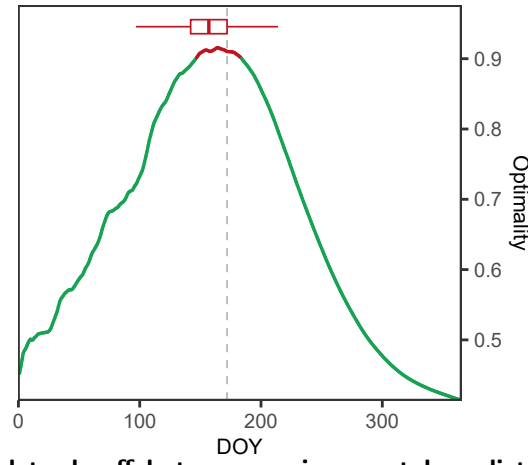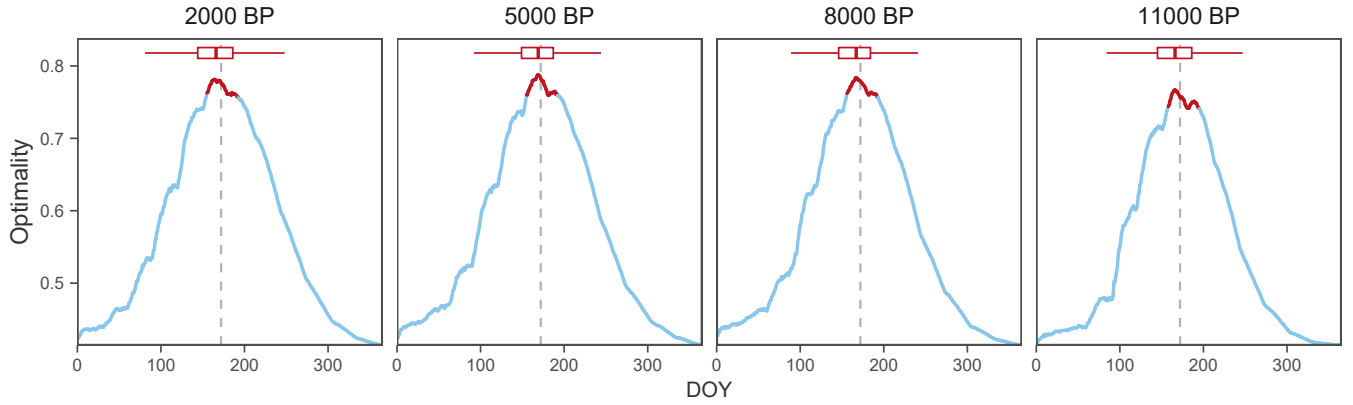
**Figure S1: Workflow of the optimality analysis for one site in Southern Europe.**

Figure S2: Average optimal trade-off between environmental predictability and growth potential across Europe, with an alternative GDD definition ($T_{lower} = 0°$C and $T_{upper} = 40°$C).

Figure S3: The average optimal trade-off between environmental predictability and growth potential is relatively stable across the Holocene. Daily mean temperatures were obtained from Van der Meersch et al. (2024), in which daily data were generated with the GWGEN weather generator (Sommer and Kaplan, 2017) based on monthly paleosimulations from the HadCM3B-M2.1 coupled general circulation model (Armstrong et al., 2019). BP stand for "Before Present" (i.e. 1950).
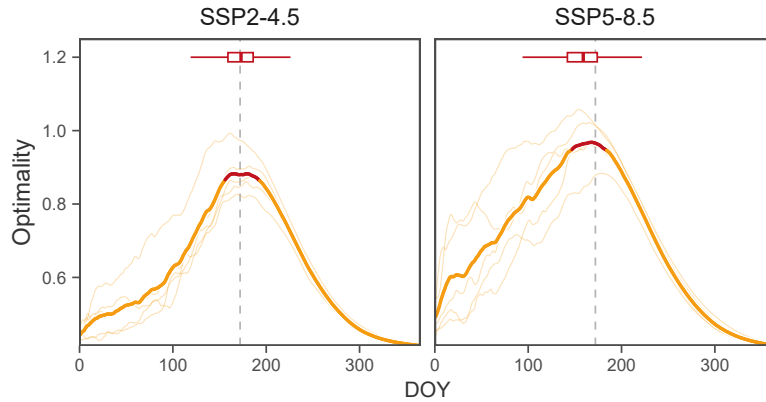
Figure S4: Average optimal trade-off between environmental predictability and growth potential in future climates (2071-2100). Daily mean temperatures came from the last Coupled Model Intercomparison Project Phase 6 (CMIP6) climate projections, for 5 global climate models (GCMs) and 2 shared socio-economic pathways (SSPs). Model projections were downscaled to a 0.1° resolution with a statistical trend-preserving method (the cumulative distribution function transform), using the ERA5-Land reanalysis as a reference observational dataset between 1981 and 2010 (Noël et al., 2022). Thin lines represent the five GCMs (GFDL-ESM4, IPSL-CM6A-LR, MPI-ESM1-2-HR, MRI-ESM2-0 and UKESM1-0-LL), large lines represent the average across GCMs.
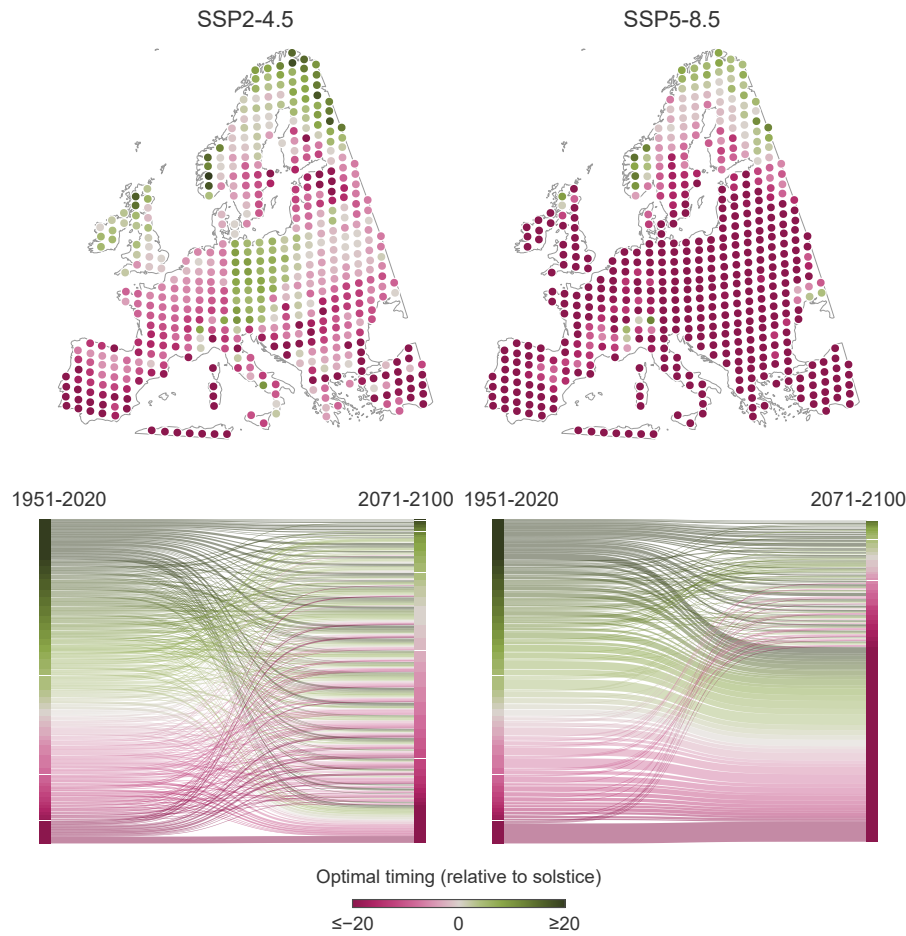
Figure S5: Average optimal timing (Figure S4) hides variation in optimal timing across the different future climatic conditions of Europe (2071-2100). On the top panel, sites are sampled on a regular grid across Europe. On the bottom panel, Sankey diagrams show the proportional flow of (site-specific) optimal timing from 1951-2020 to 2071-2100. Colors indicate the timing—relative to the solstice—of the median optimal day.

References

Armstrong, E., P. O. Hopcroft, and P. J. Valdes. 2019. A simulated Northern Hemisphere terrestrial climate dataset for the past 60,000 years. Scientific Data 6:265.

Hijmans, R. J. 2024. terra: Spatial Data Analysis. R package version 1.8-6,.

McMaster, G. S., and W. W. Wilhelm. 1997. Growing degree-days: one equation, two interpretations. Agricultural and Forest Meteorology 87:291–300.

Muñoz Sabater, J., E. Dutra, A. Agustí-Panareda, C. Albergel, G. Arduini, G. Balsamo, S. Boussetta, M. Choulga, S. Harrigan, H. Hersbach, B. Martens, D. G. Miralles, M. Piles, N. J. Rodríguez-Fernández, E. Zsoter, C. Buontempo, and J.-N. Thépaut. 2021. ERA5-Land: a state-of-the-art global reanalysis dataset for land applications. Earth System Science Data 13:4349–4383.

Noël, T., H. Loukos, D. Defrance, M. Vrac, and G. Levavasseur. 2022. Extending the global high-resolution downscaled projections dataset to include CMIP6 projections at increased resolution coherent with the ERA5-Land reanalysis. Data in Brief 45:108669.

Sommer, P. S., and J. O. Kaplan. 2017. A globally calibrated scheme for generating daily meteorology from monthly statistics: Global-wgen (gwgen) v1.0. Geoscientific Model Development 10:3771–3791.

Van der Meersch, V., E. Armstrong, F. Mouillot, A. Duputié, H. Davi, F. Saltré, and I. Chuine. 2024. Biological mechanisms are necessary to improve projections of species range shifts. bioRxiv .